LA-UR-19-29556
Approved for public release; distribution is unlimited.

Title: Modeling of Pyroprocessing Hot Cell for Process Monitoring Evaluation

Author(s): Lafreniere, Philip Leo
Tutt, James Robert
Fugate, Michael Lynn
Key, Brian P.

Intended for: Report

Issued: 2019-09-23

Modeling of Pyroprocessing Hot Cell for Process Monitoring Evaluation

Philip Lafreniere, James Tutt, Mike Fugate, and Brian Key

Los Alamos National Laboratory

September 11, 2019

1. Introduction

In this report, we examine studies undertaken to determine the applicability of applying measurements with a neutron counter within a pyroprocessing hot cell. The studies focus on the modeling of the hot cell and neutron counter in Monte Carlo N- Particle Code (MCNP) to determine expected radiation effects and applicability of neutron counters. The neutron counter of focus was the High Dose Neutron Detector (HDND) developed at Los Alamos National Laboratory (LANL) [1]. We studied the HDND to determine what would be the detector response under normal background conditions with operating process equipment as well as the background's potential effect on counting applications involving a U/TRU ingot produced by the pyroprocessing electrorefiner. To perform this task, we were required to develop models of the pyroprocessing process cell and unit operations and generate source terms for various different times in the process. The data for the pyroprocessing materials came from SNL's Safeguards and Security Process Model (SSPM) as part of MPACT's advanced integration mission [2]. This report will discuss the development of the pyroprocessing process cell and unit operations models in MCNP as well as various simulations to determine the applicability of the HDND for process monitoring efforts in the hot cell.

2. Modeling of Pyroprocessing Hot Cell

The focus of the modeling was specifically on the process cell of the pyroprocessing facility with no focus on the fuel fabrication cell or additional post-process storage cells. We developed the process cell utilizing information available from previous efforts in facility development and unit operations design using openly available sources. Specifically for determining the dimensions and layout of the process cell, information was taken from the efforts in the development of a pilot-scale pyroprocessing facility developed by the Argonne National Laboratory (ANL) and commercial partner Merrick & Company [2]. In addition, patent documents and past reports from the fuel conditioning facility (FCF) at the Idaho National Laboratory (INL) were studied and applied.

To model the facility, we simplified our flow sheet for our analysis and layout of the facility. A representation of this simplified flow sheet is seen in Figure 1. As seen in the flowsheet, the process cell has been reduced to its core processes. The electroreducer where the oxide fuel is processed contains a neutron source in terms of the anode basket placed within it during operation. The reduced fuel is transferred to the electrorefiner. Here, a source of neutrons takes several forms: the anode baskets and liquid cadmium cathode when operating as well as the salt always contains actinides in a near steady state thus contributing a constant source of background neutrons in the salt. The transferred product is then processed by the U and U/TRU processors whose ingots as well as distilled process salt are a notable neutron source. Finally, we simplified the drawdown processes into a single piece of unit operation equipment where the processed salt produces a neutron source in the process cell.

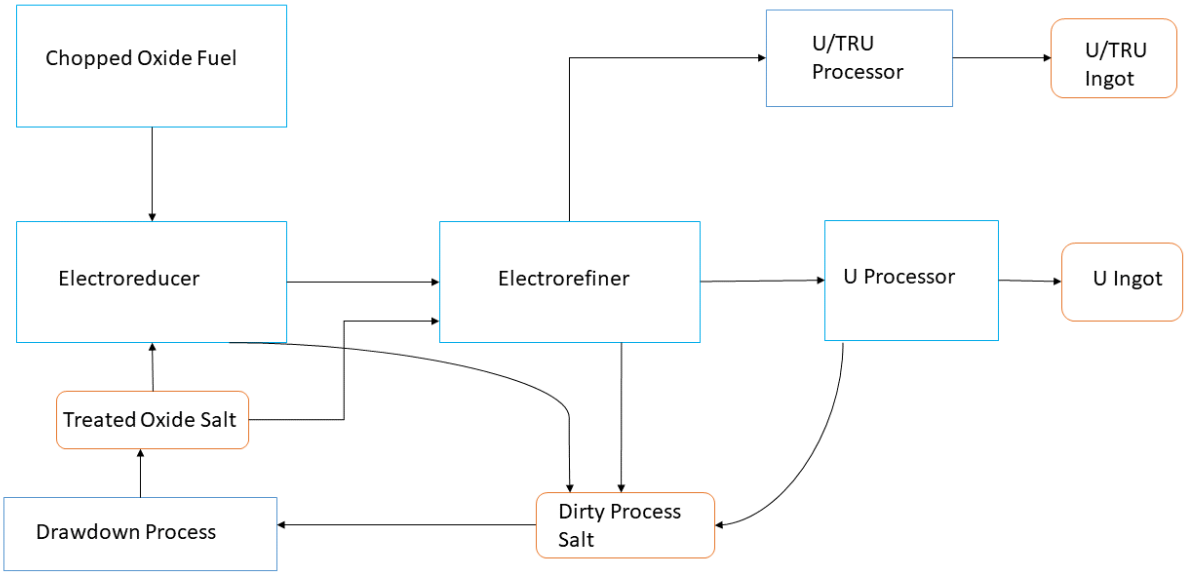

Figure 1- Simplified Flow Sheet for Pyroprocessing Process Cell Modeling

The subsequent subsections document the assumptions and descriptions of the modeled unit operations in MCNP.

2.1 Assumptions of Electrorefiner Modeling

The modeling in MCNP of the electrorefiner is based off of several assumptions for both the dimensions of the electrorefiner as well as the composition of the salt bath. The design of the facility and with it the electrorefiner is based off a pilot-scale facility developed by ANL and commercial partner Merrick & Company [2]. The electrorefiner itself is based primarily off the design developed at ANL [3]. This design involves an arrangement of cylindrical cathodes and planar anode baskets in sequence that can be arranged based off of throughput. These electrodes are suspended in a LiCl-KCl bath over a conveyor belt to catch and extract scraped dendrites from the cathodes during operation to increase throughput and maintain current density in the

system. The electrorefiner is rectangular parallelepiped and placed within an argon atmosphere process cell.

The first thing required to model the electro refiner in the process cell in MCNP is to develop assumptions given how it is simplified and represented in the model. To do so, the dimensions of the electrorefiner were determined. To do this, drawings from papers and patents were assumed to be to scale though they were never specifically stated to be so. What was specifically needed for the modeling was general assumptions for modeling the arrangement of planar electrodes in the ER and how they may align proportionally to the greater vessel. As actual dimensions were not available, developing a model that best mimicked this geometry was the priority and the models developed do reproduce this.

The drawing of the pilot-scale facility operating floor was analyzed based off of stated dimensions to estimate dimensions of the process cell and the length and width of the electrorefiner [3]. Further analysis of electrorefiner patent information was used to determine depth of both the salt bath and the equipment itself [4]. A summary of final dimension estimates derived from this process is provided in Table I.

Table I- Dimensions of Modeled Electrorefiner

Dimension	Estimated Size
Length	3.38 meters
Width	1.5 meters
Depth of Salt Bath Holder	2.04 meters
Depth of ER Equipment	2.55 meters
Volume of ER Bath Holder	10.3 cubic meters

The next step was to determine the composition of the salt bath. Composition of the salt bath versus time was provided by Sandia National Laboratories (SNL) through the SSPM-EChem

systems model developed as part of the MPACT campaign [2]. Data provided by SNL gave a metal composition in the salt. However, the data received had no details about the eutectic composition of the salt, a key requirement for accurate MCNP modeling. To do this, the first step was determining the concentration of metal chloride salts given the provided metal composition data. To do so, it was assumed all metal composition in the salt composition data was in metal chloride form and bonded only to the most common valence state. Thus, the number of moles of each metal was determined as the data was provided in kg, and from this molar data the number of moles of chlorine in salt attached to the metal chlorides could be determined. From this molar content of chlorine, the mass of chlorine in the salt could be determined. Knowing the mass of chlorine metal chlorides allowed for the calculation of the total mass of metal chlorides in the bath.

Knowing the metal chlorides mass, an assumption of the weight percentage of LiCl-KCl salt in the salt bath needed to be made. Past reports and papers indicated the composition and density of the Mark-IV electrorefiner at the fuel conditioning facility (FCF) processing EBR-II fuel at INL [5]. This past analysis indicated that LiCl-KCL having treated 205 kg heavy metal comprises a weight percentage of 77.77% in the eutectic. Of course, within the context of the modeled electrorefiner, the arrangement and composition of the salt will likely be different. However, it is necessary to keep the concentration of LiCl-KCl high, including through periodic addition of LiCl-KCl salt to the electrorefiner. Thus a weight percentage of LiCl-KCl between 75 and 80% is a fair assumption. In addition, an assumption about the depth of the salt within the electrorefiner is assumed to be 1/3 of the total salt bath holder depth. This assumption, like that of the weight percentage of LiCl-KCl salt, is based off of past experience with the Mark-IV electrorefiner [6]. This leads to a eutectic salt density around 2.237 g/cm^3.

However, these drawing and dimensions were only for a design that did not include a liquid cadmium cathode (LCC). Thus, taking information from an additional computer aided drawing (CAD) of the ER featuring a set of 4 LCC's, the width of the ER was modified to accommodate four LCC's [2]. Additional width was defined to accommodate a large volume beryllia crucible to hold the liquid cadmium for the LCC. Beryllia was chosen as past experience demonstrated its use for this purpose in the Mark-IV [7]. The standard dimensions of possible crucible candidates was taken from data from a crucible handbook published by Oak Ridge National Laboratory (ORNL) [8]. However, as far as the model, other materials can be substituted in for beryllia with ease due to the nature of materials in MCNP. With these crucibles added the total width of the modeled ER is 1.61 meters compared to the previous 1.5 meters.

A visualization of this model is seen in Figure 2.

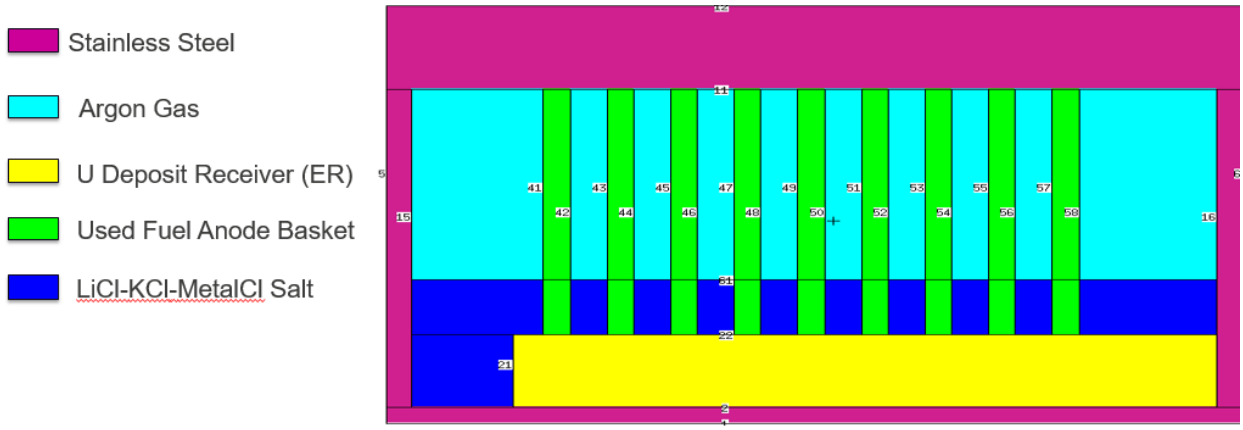

Figure 2- Electrorefiner MCNP Model

2.2 Assumptions of Uranium Cathode Processor Modeling

Assumptions regarding the uranium cathode processor were primarily based off of information from the uranium cathode processor (CP) at the FCF at INL. Using data from previous papers about the CP, dimensions of the geometry and materials were determined [9]. The vessel of the CP was assumed to be made of steel and consisting of an inner and outer chamber to contain the heating elements of the inner chamber. The CP was modeled as having two crucibles. One at the bottom and center of the inner chamber to contain distilled salt is made of stainless steel. Elevated above it on a tantalum platform is a second crucible made of graphite containing the U product. The crucible selected is based off a standard crucible that is able to contain the volume of U dendrites from the data provided from SNL. These dimensions are based off standard dimensions from the crucible handbook at ORNL [8].The crucible has a wall thicknesses of 3.75 centimeters and has too regions for consolidation due to requiring a bilge for handling. The inner diameter of the lower and smaller volume region is 13.07 centimeters while the upper larger volume region has a radius of 15.875 centimeters.

Between these two crucible is a conical tantalum radiation shield. Each layer of steel for both the inner and outer chamber contains a thin copper lining. The height of the crucible above the floor of the hot cell is 2.6 meters as determined from being slightly taller than the modeled electrorefiner. The total vessel height is 3.21 meters as to keep the same ratio of height of crucible to vessel as in the FCF facility. Total radii of the inner and outer chambers were determined by inspecting dimensions from the ANL report as was done for the electrorefiner dimensions [2]. This came to an inner chamber radius of 42.77 centimeters and an outer chamber radius of 75 centimeters. The thickness of the walls of each chamber as well as copper lining were adapted from the data for the CP at INL consisting of thicknesses of 0.32 and 0.3175

centimeters respectively. The atmosphere of the cathode processor while is assumed to be argon like the rest of the hot cell. During a simulated CP operation, the graphite crucible contains the U product and the steel crucible contains distilled ER salt.

A visualization of this model is seen in Figure 3.

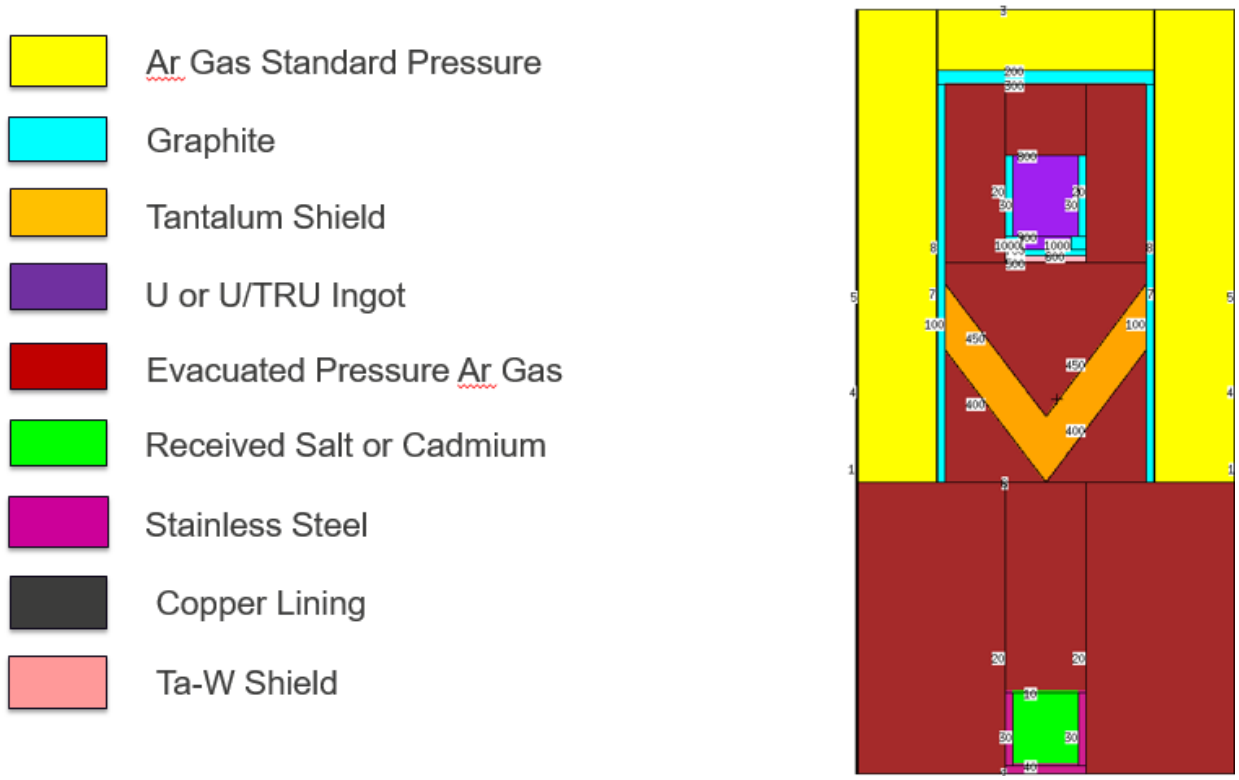

Figure 3- Cathode Processor MCNP Model

2.3 Assumptions of Electroreducer Model in Hot Cell

To model the electroreducer hot cell, a small set of assumptions were made. The model was assumed to be that of the planar electrorefiner modeled before. The only difference being that the eutectic salt would not be LiCl-KCL but solely LiCl as is common with electroreducer design. Besides this, the assumptions of the dimensions of the equipment are the same, consisting of

planar baskets submerged in a eutectic salt with a rectangular parallelepiped serving as the vessel.

2.4 Assumptions of Modeling U/TRU Processor

The U/TRU processor like the electroreducer is an adaptation of another unit operation model in this case the U cathode processor. The difference being only what materials are present. Rather than ER salt being present in the lower receiving crucible, it instead contains liquid cadmium that has been distilled off from the crucible in the raised platform. In addition, due to the reduction in total mass, the crucible contains the U/TRU product only in the lower region of the crucible while the remainder is filled with the vacuum evacuated gas in the upper region of the crucible. The remainder of the dimensions and materials are identical to the cathode processor.

2.5 Assumptions of Modeling Drawdown Processes

From our current flowsheet, the pyroprocessing process consists of four drawdown operations. These operations are the salt purification, oxidant production, UTRU drawdown/electrowinning, and fission product drawdown. These four processes are assumed to be combined in one process within our model. The drawdown equipment is modeled as an upright cylinder with the same assumptions for salt density and thus level as previously made for the electrorefiner. Due to the combination of several different process, salt is always present in the process however it exists in different levels and masses depending on what drawdown steps are integrated. The upright cylinder itself is 9.86 centimeters thick steel with an inner radius of 29.34 centimeters. The total height is 250 centimeters.

2.6 Arrangement of Unit Operations in Modeled Process Cell

The process cell was modeled integrating all of these individual unit operation models previously described. The layout of the unit operations and their positions were determined from the same drawing for a pilot-scale plant from which the assumptions about unit operations dimension come from. The total dimensions of the cell are 27.57 meters x 10.4 meters x 500 meters with wall thicknesses of 1.25 meters of concrete. The atmosphere of the cell is assumed to be pure argon with concentration of 80 ppm. A drawing of the layout with the unit operations placed and labeled are seen in Figure 4.

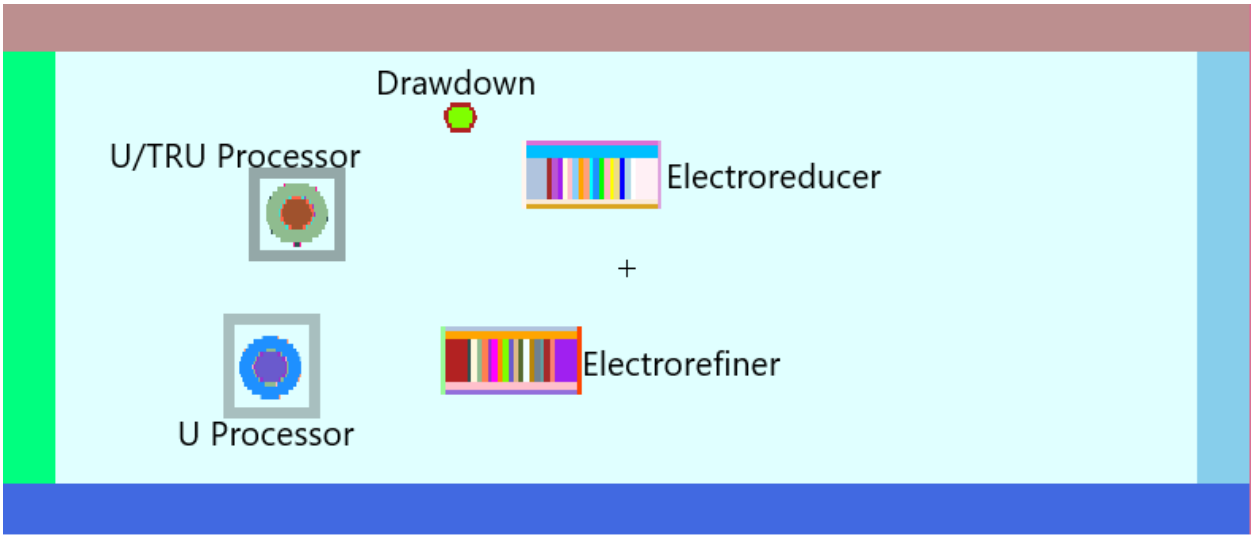

Figure 4- Layout of Hot Cell with Unit Operations in MCNP

3. Determination of Source Terms

Materials that move throughout the pyroprocessing hot cell produce radiation, especially neutrons. The source of these neutrons depends on the environment that the source is being measured. Across all unit operations, where actinides are present there is a source of spontaneous fission neutrons, thus this source must be accounted for at all unit operations. In addition, due to the presence of LiCl and LiCl-KCl salts due to the presence of especially Li-7, the contribution

of (alpha,n) neutron interactions as a source must also be factored in. To calculate these source terms from both contributing sources, the software package SOURCES-4C is applied [11]. To do this, the composition of each material of interest is read in and assumed to be homogenous. This composition is comprised of the major alpha emitters, spontaneous fission neutron emitters, and target isotopes such as Li-7 and Cl-32 that would be present to produce (alpha,n) reactions. With these compositions of the material, SOURCES-4C can calculate the spontaneous fission source, (alpha,n) source, and the total combined source as well as neutron energy spectrum for a selected number energy group between specified bounds.

3.1 Source Term Calculations: Movement of Material over Time

The material compositions for each unit operation in the pyroprocessing hot cell was calculated by the SSPM- Echem model and consisted of both isotopic fractions and masses of each element. Compositions were reported in hourly increments from 5980 to 6480 hours of operation, giving a 500 hour period under which the facility is assumed to be in steady state operation. A 25 hour snapshot of this period was taken between hours 6456 and 6480 to analyze material flow through the facility and the associated radiation signatures as a function of time and position. A plot of the total U/TRU mass moved over this time period is shown in Figure 5 and segregated by the unit operation in which the material is present.

As demonstrated in the plot, the amount of U/TRU present within unit operations fluctuates with time. When not in unit operations, material is either in storage awaiting processing outside the process cell, in movement within the hot cell, or in finalized ingots moved to storage in fuel storage and processing cell. We assume this material is adequately shielded in any of these three cases and that the only neutron flux present is contributed by material currently being processed in unit operations.

There is always a presence of U/TRU products in the ER and OR salts with the ER being substantially greater. The OR anode is placed within the cell for the majority of this period, except for two hours of down time (6458 and 6459) where products are being removed to be moved to the ER. The ER anode is inserted at time 6458 and is essentially exhausted of U/TRU material by hour 6465 where it is still present until hour 6474 at which point it is removed and replaced at hour 6480. The LCC operates between hours 6459 and 6466. It is present for less time compared to the anode as the amount of material processed is less. Finally The U cathode processor operates between hours 6465 and 6470 while the U/TRU cathode processor operates between hours 6465 and 6469. The presence of TRU is greater in the U/TRU cathode processor, though the total U/TRU mass is greater in the U processor with the majority of it being uranium.

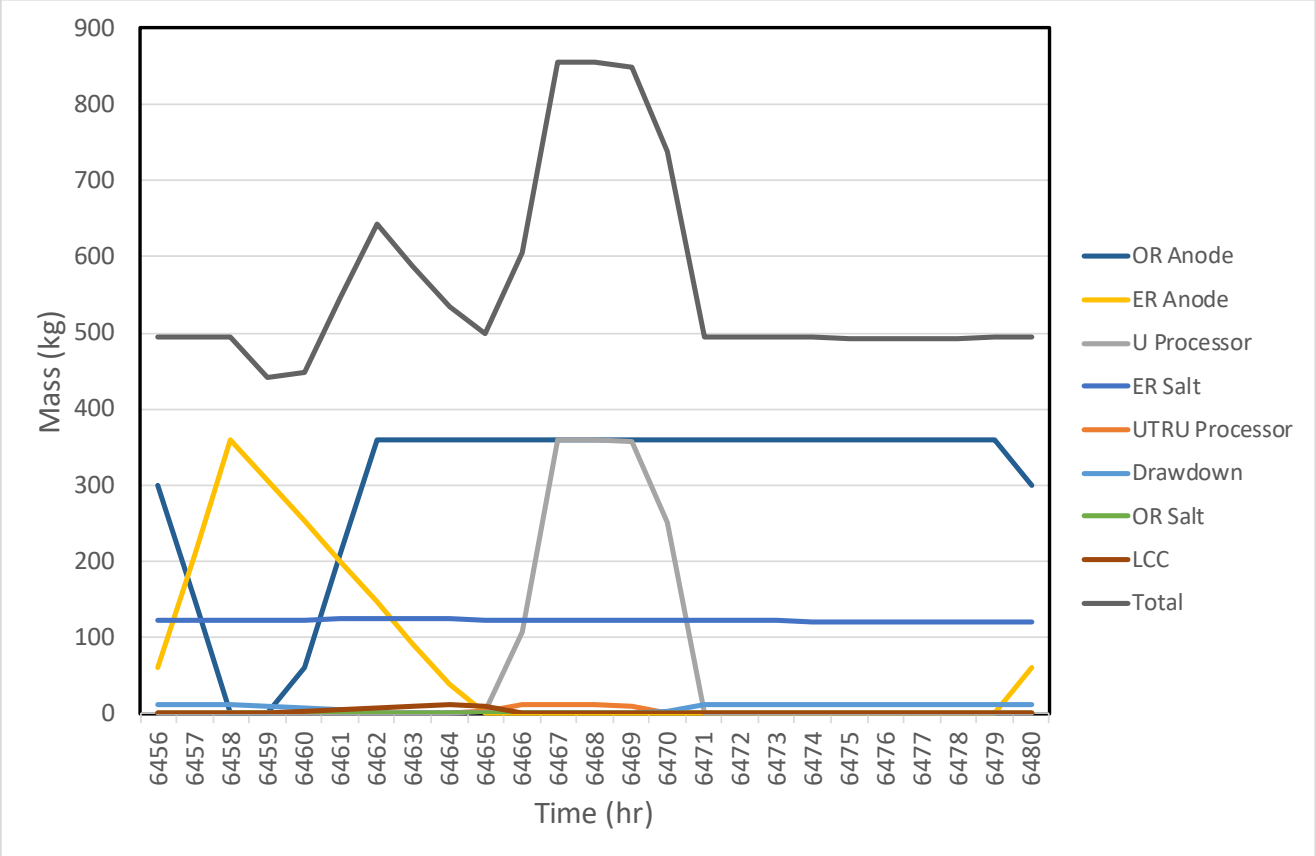

Figure 5- Movement of U/TRU Mass vs Time

3.2 Source Term Calculations: Hot Cell Simulations

Neutron source terms were calculated using the time series data for each time between 6456 and 6480. These calculated source terms consisted of neutron intensity in terms of n/cm^3-s for both the spontaneous fission and (alpha,n) neutrons as well as energy distribution divided into 50 probabilistic bins between 0 and 10 MeV. A plot of the total neutron source rate and the neutron source rate for each unit operation is seen in Figure 6.

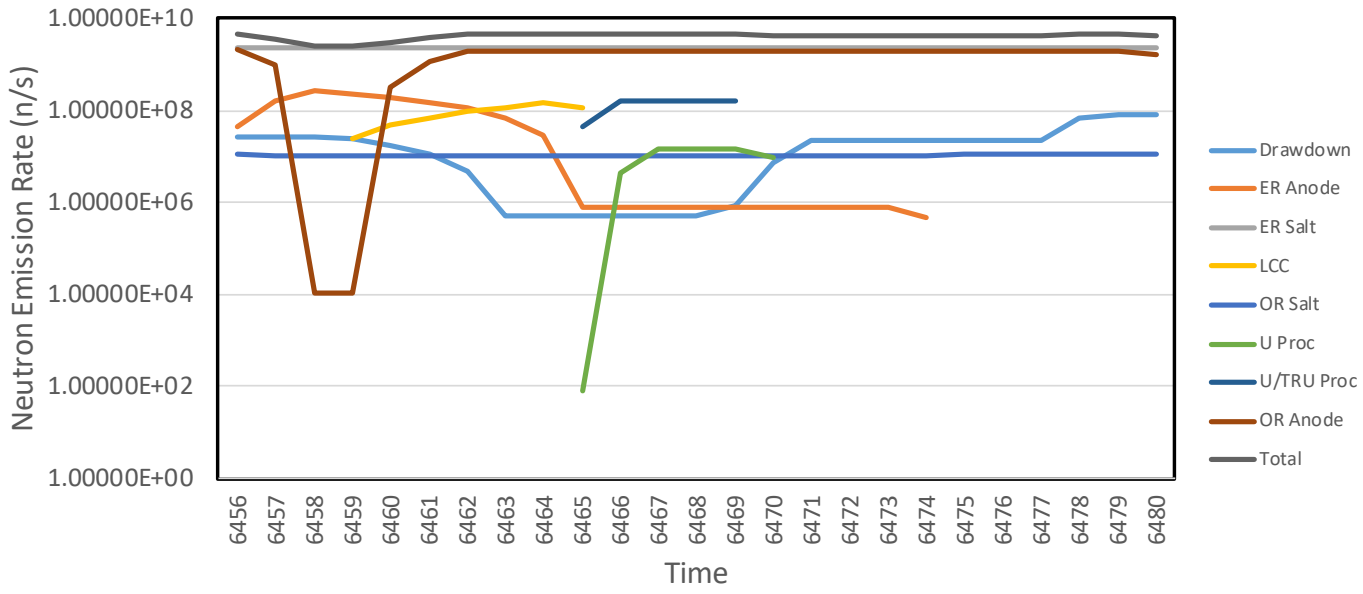

Figure 6- Total Neutron Emission Rate vs Time

As demonstrated by the plot, the majority of neutron activity comes from the ER Salt and the OR anode. This is because of the increased level of (alpha,n) interactions, especially in the OR anode where the interaction of alphas with oxygen 18 atoms produces a strong source neutrons. Within the drawdown and ER, interaction of alphas with Li and Cl in the LiCl-KCL eutectic salt produce a significant source of (alpha,n) neutrons. The ER anode source is not as significant due to a reduction in low-z target atoms as compared with the OR anode. The source terms for each individual unit operation follows the same trends as their U/TRU movement from Figure 6. With

increased presence of U/TRU there is a correlating neutron source. However, the total source does not follow the same trend as it is dominated by the source from the ER salt. It only dips during times 6458 and 6459 when the anode baskets are being removed for ER processing as it removes the other major source of neutrons in the hot cell.

Knowing the intensity of the individual neutron sources from the unit operations, the neutron source was integrated into the MCNP file probabilistically using cell reduction where the probability of a cell being sampled for the source neutron was determined by its intensity divided by the total intensity of the background neutron source. After selection of the sampled cell, the script then samples from the generated energy distribution for the neutrons in that cell.

4 Radiation Counting Modeling

Several modeling campaigns were undertaken to determine the effects of radiation in the process cell and their affect and applicability from a process monitoring perspective.

4.1 Hot Cell Simulations: Flux Tallies

The first simulation campaign undertaken with was to determine what the neutron flux profile throughout the cell was. This was performed via the application of an FMESH 4 tally with 250 equally spaced mesh elements in the x and y direction and one mesh element in the z direction which results in a total of 250^2 mesh points throughout the cell. Tallied fluxes in each grid element can be presented in plotted form via MCPLOT. This simulation was performed for each time step between 6456 and 6480. Figures 7 through 14 provide the visual plots of these tallies.

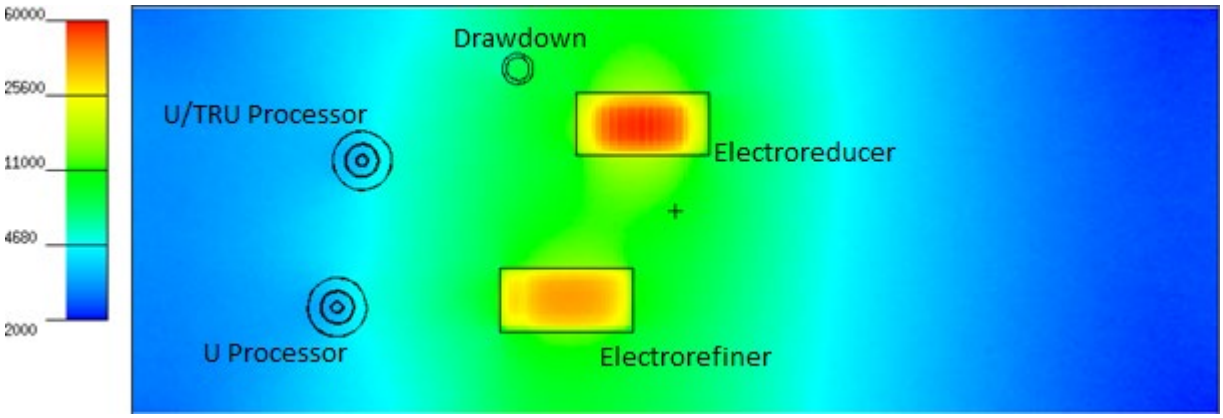

Figure 7- Neutron Flux Profile Time 6456 (Units of legend n/cm^2-s)

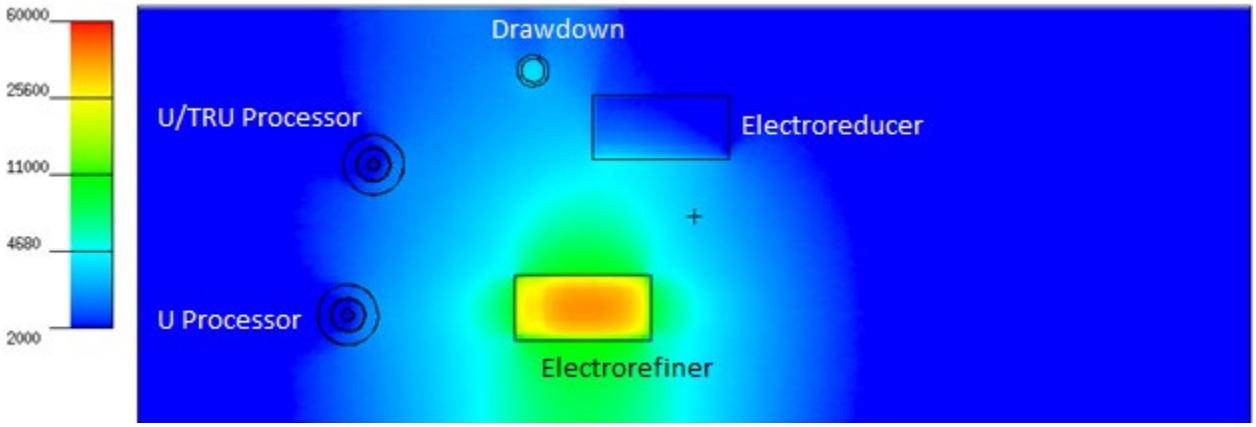

Figure 8- Neutron Flux Profile Time 6458 (Units of legend n/cm^2-s)

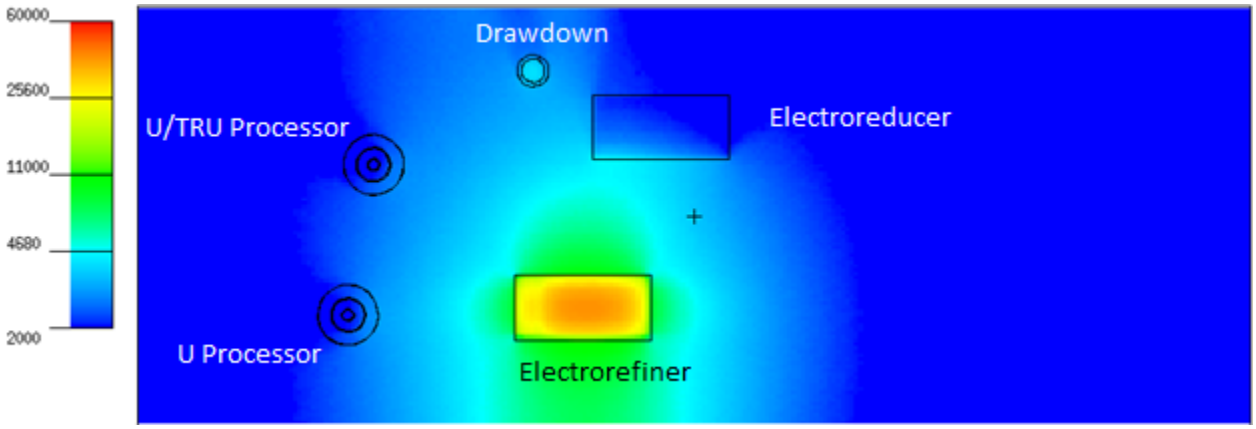

Figure 9- Neutron Flux Prolife Time 6460 (Units of legend n/cm^2-s)

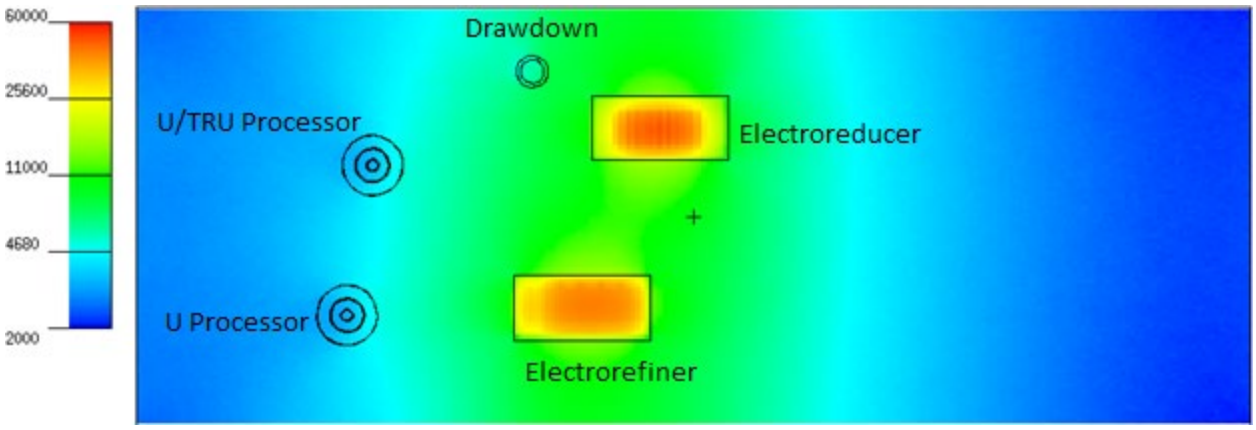

Figure 10- Neutron Flux Profile Time 6462 (Units of legend n/cm^2-s)

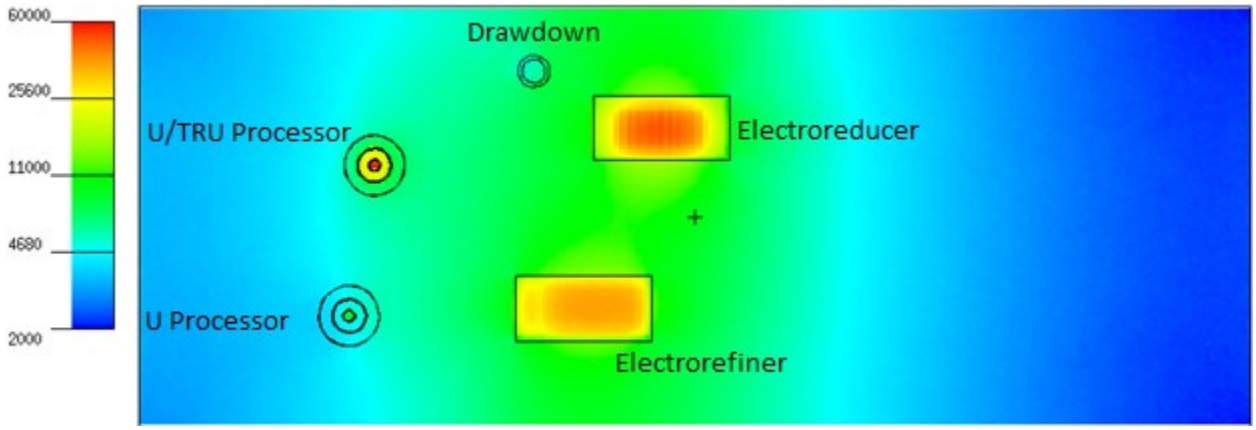

Figure 11- Neutron Flux Profile Time 6466 (Units of legend n/cm^2-s)

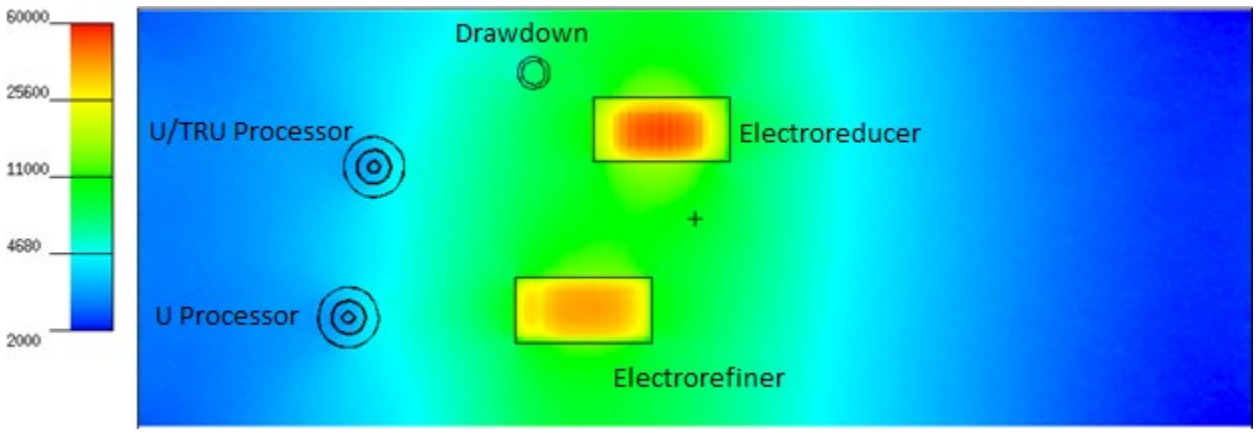

Figure 12- Neutron Flux Profile Time 6471 (Units of legend n/cm^2-s)

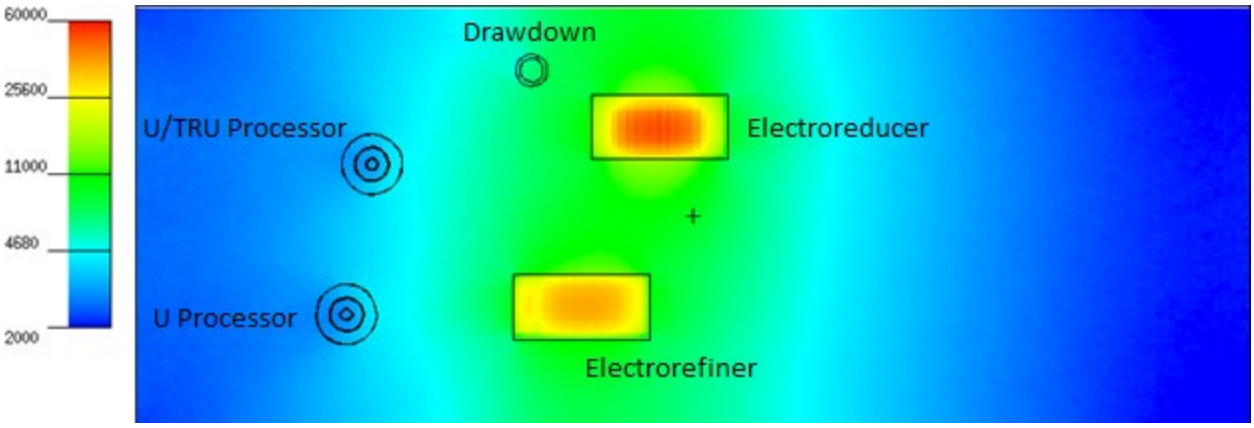

Figure 13- Neutron Flux Profile Time 6475 (Units of legend n/cm^2-s)

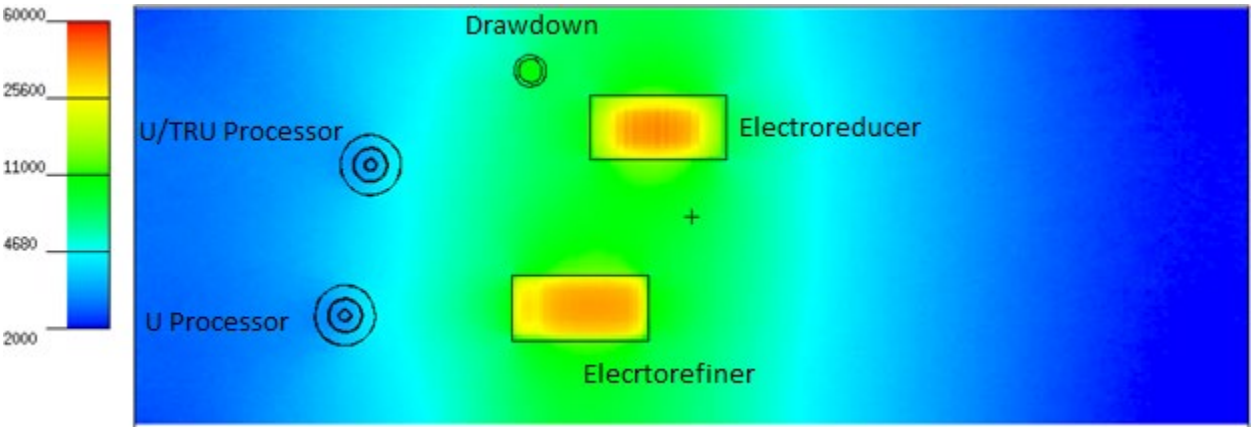

Figure 14- Neutron Flux Profile Time 6480 (Units of legend n/cm^2-s)

Beginning at time 6456, the neutron flux is dominated by the ER and electroreducer as expected. At time 6458, no substantial source is coming from the electroreducer as the anode has been removed while the salt in the ER still gives off the same strong source of neutrons. At time 6460, the reinsertion of the anode baskets in the OR results in the return of the source, though weakly, from the OR anodes. At time 6462, the baskets are fully inserted and the primary sources are again from the ER and OR. At time 6466, the U and U/TRU processors are at the peak of their metal processing resulting in a noticeable flux coming from the processing equipment. At times 6471 and 6475, we see the continued processing of the fuel with removal of ER anodes, leading

to little change in the flux from the ER as it is dominated by the actinides in the salt as the source of neutrons. At time 6480, the OR process is reaching completion and the anodes are being removed from the salt seeing yet again a reduction in flux from the OR.

4.2 Hot Cell Simulations: High Dose Neutron Detector Background Counting Investigation

The next set of simulations performed was to determine the neutron counts incident on LANL's high dose neutron counter (HDND) if it was to be placed at various positions on the floor of the hot cell. The HDND is being developed specifically for high radiation environments such as the pyroprocessing hot cell and consists of a rectangular filled array of parallel plates containing boron lined Ar+CO_2 filled tubes. There are a total of six of these parallel cells each about 0.5 centimeters thick and each are layered with 1.6 cm thick plates of polyethylene to provide neutron moderation [1]. Neutron interactions with the boron produced charged alpha particles which are then registered in the gas. The detector, as it is modeled in MCNP, is seen in Figure 15.

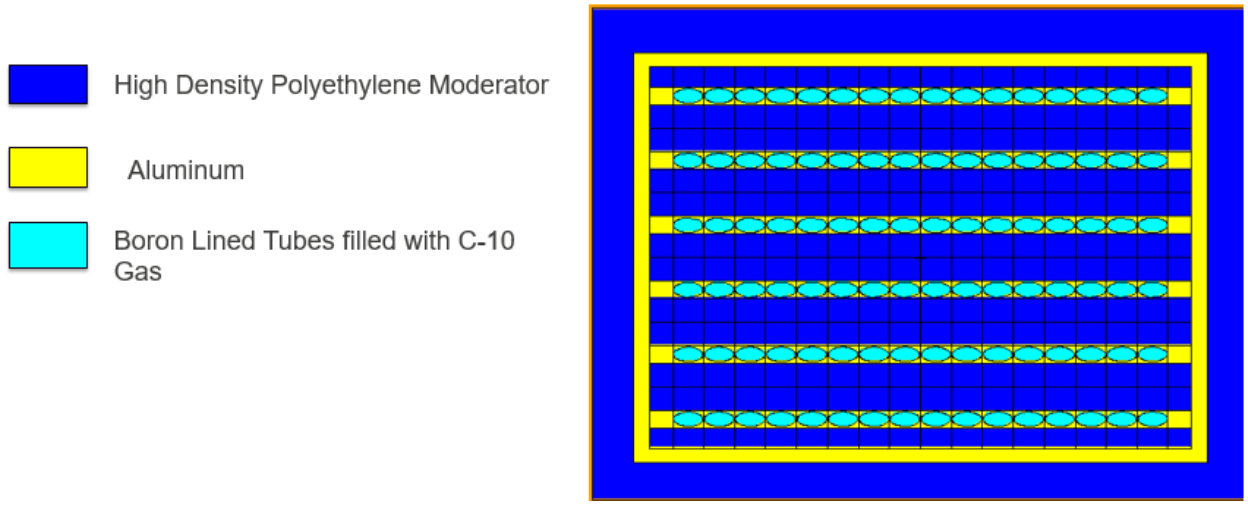

Figure 15- Top Down View of HDND Detector in MCNP

The detector is placed at six different locations within the modeled hot cell. A summary of these locations is seen in Figure 16 with the location each one numbered with relation to the hot cell.

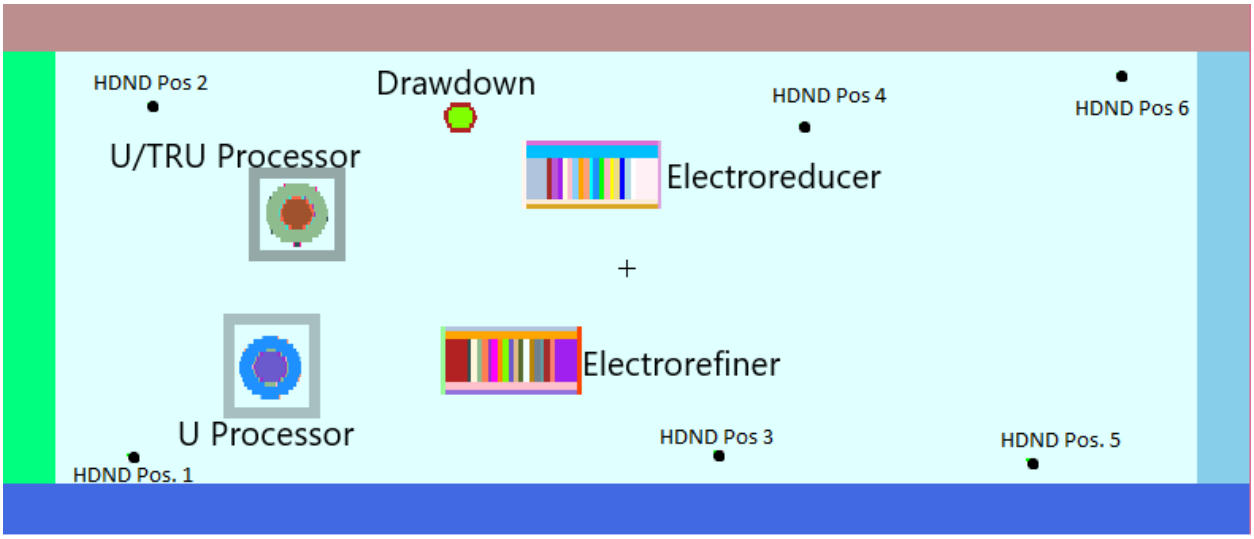

Figure 16- Modeled Hot Cell with Position of Detector Indicated

The detectors utilized FT8 tallies in MCNP to register each individual capture of neutrons and subsequent alpha production. Results of these tallies are multiplied by the total emission rate to determine total background rate in the HDND in counts per seconds. The final results for the 25 different time cases at the six different positons are seen in Figure 17.

The results of these background calculations demonstrate several key takeaways. First, the greatest background count rates are present at positions 3 and 4 indicating that total number of background counts is related to the distance from the ER and the OR. As one might expect, the lowest background count rates come from positions 5 and 6 which are the furthest distance away from the processing equipment. This shows that for counting measurements to occur in cell, shielding the process equipment or an informed selection of detector placement will producing better counting conditions. In addition, the counting rates for each position all follow the same

trends over the course of the 25 hour period. The count rate first decreases substantially due to the removal of anodes from the OR significantly decreasing the neutron flux in the cell. It then increases as the OR anodes are replaced and levels out with the exception at time 6469 where there is a small peak. This is the time when both processors are operating as well as the ER and OR increasing the total neutron flux to its maximum, increasing the count rate. However, the amplitude of this counting peak may not be substantial enough for a process monitoring purpose.

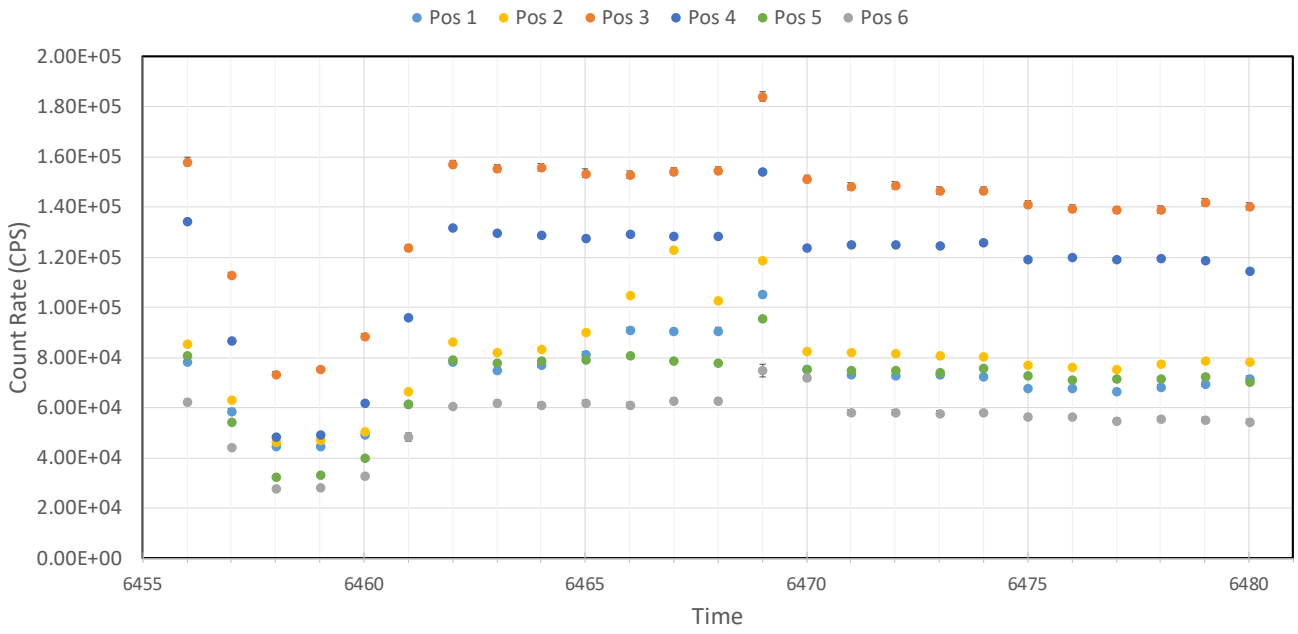

Figure 17- Weighted Background Tally Results

4.3 Hot Cell Simulations: Measurement of Ingot in Hot Cell

With a sense of background count rate determined, additional simulations were undertaken to measure a U/TRU product form the electrorefiner at all six detector positions in the presence of the background neutron radiation in the hot cell. In addition, this U/TRU ingot has a mass of approximately 13 kg of heavy metal and is counted at a distance of 20 cm from the HDND. This

ingot mass was taken directly from the data for U/TRU output mass in the SSPM model. This U/TRU product contained isotopes from all major actinides between U and Cf. Most importantly contains a notable concentration of Cm thus resulting in a strong neutron source of 1.61×10^8 neutrons/second which is roughly 3.6 percent of the total neutron emission rate of all neutron sources in the hot cell.

Like with the background studies, FT8 capture tallies were utilized to determine rate of neutron capture using analog Monte Carlo. However, the tallies were tuned so that the capture rate could be measured in terms of both total capture as well as capture from individual source cells. This allows discrimination captures by neutrons originating from the ingot and those that come from background sources. This was performed by using a SCD card in MCNP specified in the user information tally to account only for a specific cell from which the source neutron came from. This method also required that for an accurate account of total background, a large number of histories had to be run. The simulations were run with enough source neutron histories to produce a relative error of less than 5% for each tally.

Simulated counts from ingot and background are seen in Figure 18. These results demonstrate that the signal coming from a U/TRU ingot will be substantially greater than noise produced by background. Thus, inspection of U/TRU ingots in situ via the application of the HDND could be possible. In addition, the results demonstrate that the signal from the ingot becomes more dominate as the distance from the electrorefiner increases. Thus, shielding design and position of measurement area should take this into effect when developing a commercial hot cell design. One curious result is that the count rates of position 1 are substantially greater than the other positions for the ingot. This is due to the positon of the detector in the corner of the cell thus experiencing a higher flux of albedo neutrons from the surrounding concrete walls. This is

another notable factor that should be taken into account when determining detector count position for in situ ingot measurements.

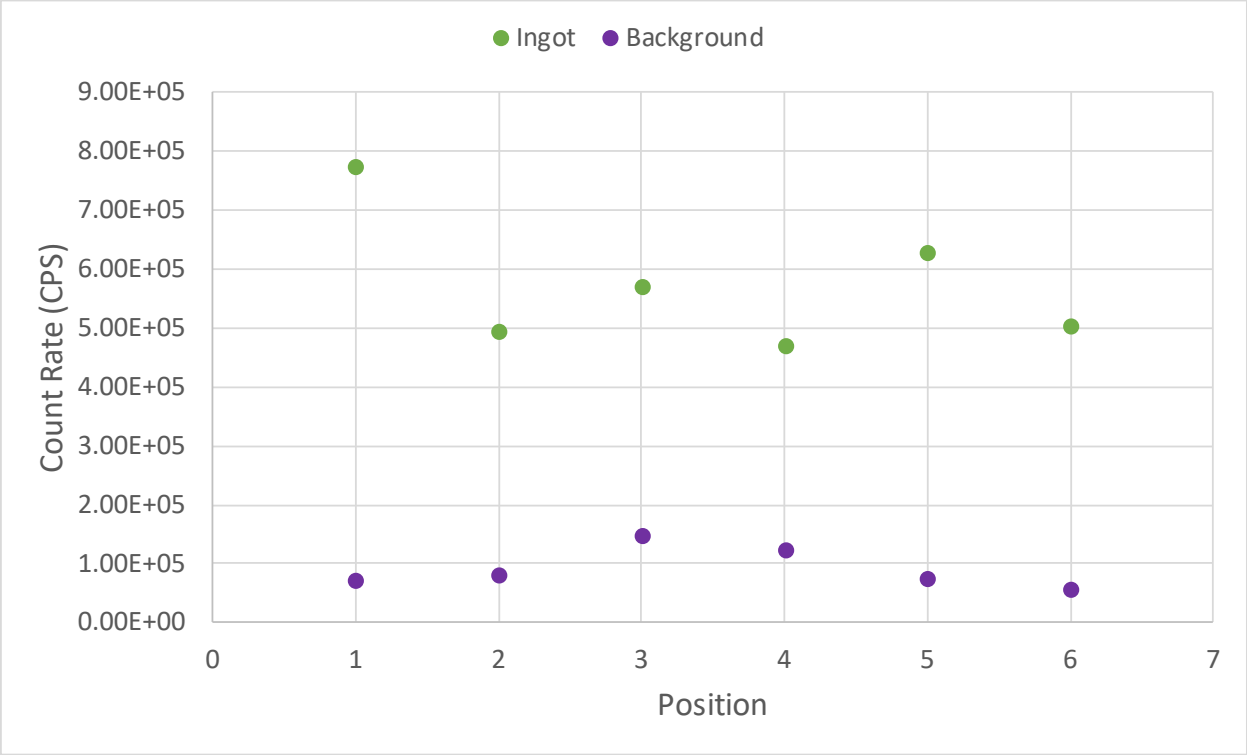

Figure 18: Count Rates vs Detector Position

In addition, studies were performed varying the mass of the ingot between 0.1 kg and the previously assumed 13 kg. These studies were performed for detectors at only positions 1, 3, and 6. The results of these studies compared to background are seen in Figure 19. These results show that, as expected, the counting rates of the ingot increase with mass. In addition, some of the lower mass count rates are close to or actually below that of the background, specifically for ingots of mass 3 kg or less. This provides valuable insight in choosing the optimum ingot size so

as to not be too large for the purpose of safeguards but also not so small as to upset the timing of operations.

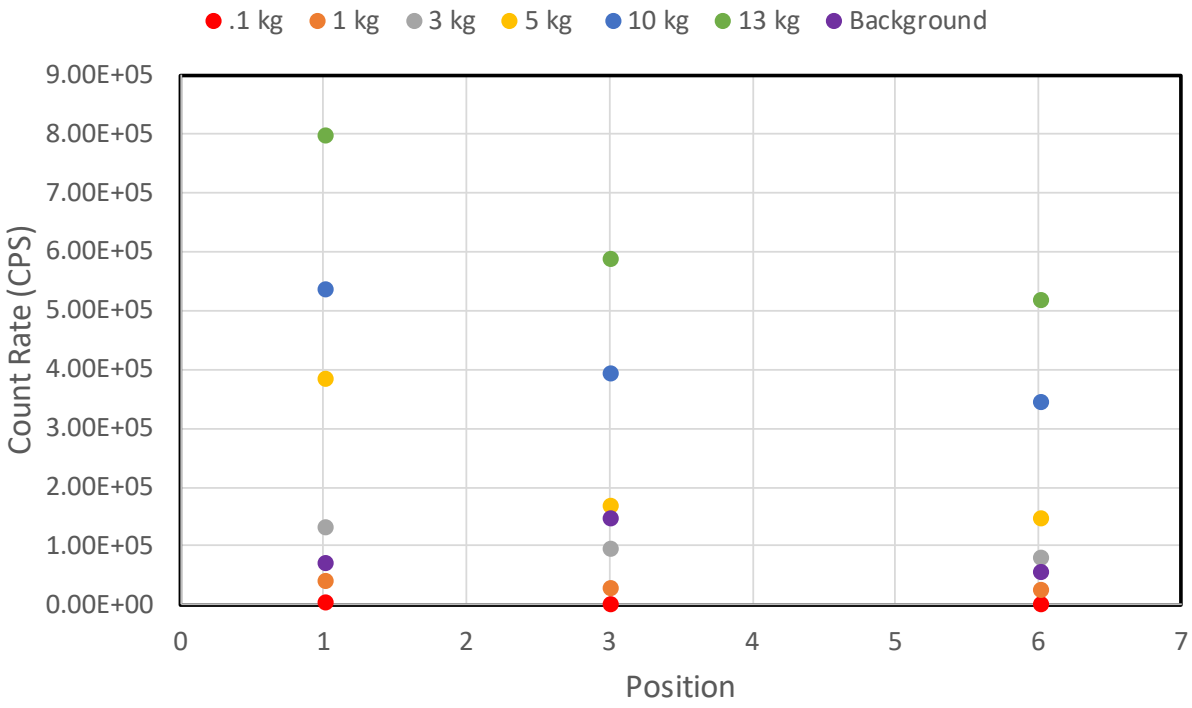

Figure 19- Count Rates vs Positon for Assorted U/TRU Ingot Masses

4.4 Hot Cell Simulations: Simulation of Gamma Flux

To best evaluate the effectiveness of the HDND in the hot cell, an establishment of expected gamma flux is necessary as gammas can also deposit energy in the detector causing a count that is indistinguishable from a true neutron count, contributing to the observed background rate. Thus, studies were undertaken to determine the dose rate from gammas at the surface of the HDND in positions 1, 3, and 6. The gamma source was calculated using the MCNP Intrinsic Source Constructor, part of the MCNPTools package included with the MCNP distribution [12, 13]. The source calculator, written in python, uses MCNP data libraries to calculate the particle emissions spectra and intensity of a given material focusing in our case on gammas. Both these

intensities and energy spectra can be then imported into the SDEF card in the same manner that neutrons were imported from the SOURCES-4C calculation using cell reduction for the relative intensities and energy spectrum probability cards.

The simulations used an F2 tally for the surface of the detector and were weighted by the total gamma intensity to determine the flux in terms of gammas/cm^2-s. In addition, a conversion factor (ICRP-21 1971) was utilized to calculate the dose rate in rem/hr from the tallied flux. The simulations were run with enough source neutron histories to produce a relative error of less than 5% for each tally. The results of these simulations for the gamma dose are shown in Figure 20.

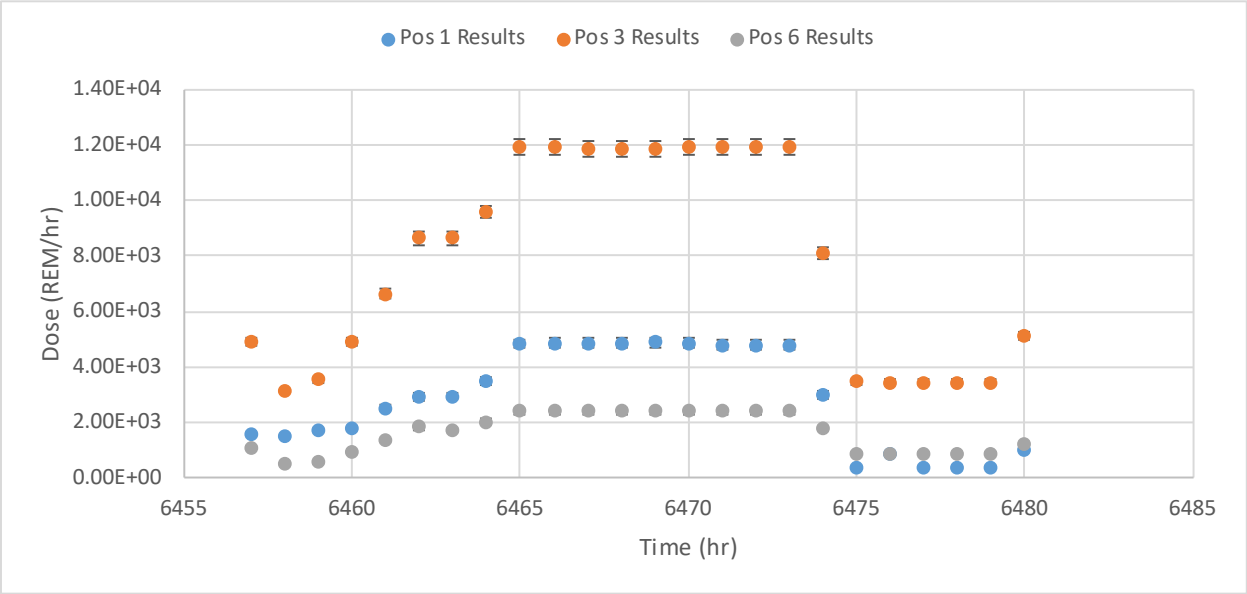

Figure 20- Gamma Dose vs Time HDND Surface

The gamma dose follows the same trend as expected as the dose is dependent on the flux. Like the neutron counts, the closer the detector is to the OR and ER the greater the dose. The only exception to this being when the dose of position 6 rises above that of position 1 during the last

six hours of operation or when the anode baskets with their residue have been removed from the ER. This could be due to the partial shielding of the detector in position 1 by the processor equipment combined with being almost equidistant from the OR as the position 6 detector. In addition, an identifiable trend is seen in which there is rise and plateau of the gamma dose when the anode is inserted and processed in the OR and the U and UTRU processors are operating. Differences during this stage are much greater than the raise during the operation of the ER in the neutron counter seen in the previous section. Given this trend, investigation of gamma monitoring may be warranted as this could be an attractive signature for monitoring radiation in the hot cell.

Next steps are to share the results of this gamma background study with the HDND team to determine the implications they will have on neutron counting efficiency in a hot cell environment.

5. Conclusions

Substantial progress has been made to develop hot cell radiation modeling in MCNP to assist the advanced integration for the virtual facility for the MPACT campaign. Taking data from systems models, source terms for neutron and gamma emission from pyroprocessing hot cell equipment have been calculated. Mapping the neutron radiation field in the hot cell has been performed in MCNP as well as studies on the effect of background neutrons, background gammas, and neutrons from U/TRU ingots in the hot cell using a simulated version of the HDND detector. Future work to be performed include integrating the mini-HDND once completed, integrating new isotopic data from the SSPM, and iterating with the HDND designers to determine the effects of the gamma dose to update our results post simulation with estimated effects on neutron counting performance.

6. References

[1] D. Henzlova and H. Menlove, "High-Dose Neutron Detector Development for Meausring Alternative Fuel Cycle Materials," in *Proceeding of Global 2017*, Seoul, 2017.

[2] Y. I. Chang and e. al., "Conceptual Design of a Pilot-Scale Pyroprocessing Facility," *Nuclear Technology,* vol. 00, no. 1, pp. 1-19, 2018.

[3] J. L. Willit and M. A. Williamson, "High Throughput Electrorefiner for Recovery of U and U/TRU Product from Spent Fuel". US Patent US 2011/0180409 A1, 28 July 2011.

[4] M. A. Williamson, S. G. Wiedemeyer, J. L. Willit, L. A. Barnes and R. J. Blaskovitz, "Bus Bar Electrical Feedthrough for Electrorefiner System". US Patent US 2013/0161091 A1, 27 June 2013.

[5] R. Mariani and D. Vaden, "Modeled salt density for nuclear material estimation in the treatment of spent nuclear fuel," *Journal of Nuclear Materials,* vol. 1, no. 404, pp. 25-32, 2010.

[6] S. Li, T. Sofu, T. Johnson and D. Laug, "Experimetnal Observations on Electrorefining Spent Nuclear Fuel in Molten LiCl-KCl/Liquid Cadmium System," Argonne National Laboratory-West, Idaho Falls, 1999.

[7] D. Vaden, S. Li, B. Westphal, K. Davies, T. Johnson and D. Pace, "Engineering-Scale Liquid Cadmium Cathode Experiments," *Nuclear Technology,* vol. 162, no. 2, pp. 124-128, 2008.

[8] M. Schwartz, G. White and C. Curtis, "Crucible Handbook: A Compilation of Data on Crucibles Used for Calcining, Sintering, Melting, and Casting," Oak Ridge National Laboratory, Oak Ridge, 1953.

[9] "Design and Development of a Cathode Processor for Electrometallurgical Treatment of Spent Nuclear Fuel," in *Proceedings of ICONE 8: 8th International Conference on Nuclear Engineering*, Baltimore, 2000.